ACS OMEGA

Open Access

http://pubs.acs.org/journal/acsodf

Article

Fabrication of Vinyl Ester-Modified Phenolic Resin Composite Coatings for the Protection of Combustible Cartridge Cases

Mengde Wu and Zhenggang Xiao*

Cite This: *ACS Omega* 2025, 10, 13807−13815

Read Online

ACCESS | Metrics & More | Article Recommendations | Supporting Information

ABSTRACT: To improve the protection of combustible cartridge cases (CCCs), four vinyl ester-modified phenolic resins (VEPRs) were prepared. Fourier transform infrared spectroscopy was used to identify the chemical structure of the coatings. Subsequently, the surface element composition of each coated sample was analyzed by X-ray photoelectron spectroscopy. The thermal properties were evaluated using thermogravimetric analysis, differential scanning calorimetry, and a heat resistance test. Additionally, the hydrophobicity of the composite coatings was examined through scanning electron microscopy, water contact angle measurement, and a salt wet test. All coated CCCs possessed excellent heat resistance. The 20 wt % VEPR-coated CCCs possessed the optimum hydrophobic property with the highest water contact angle of 112.5° and exhibited the longest heat resistance time of 111 s at 250 °C, indicating optimal performance in preventing heat from penetrating the CCCs. Therefore, the results indicate that the newly developed composite coating formulations significantly improve the protection of CCCs.

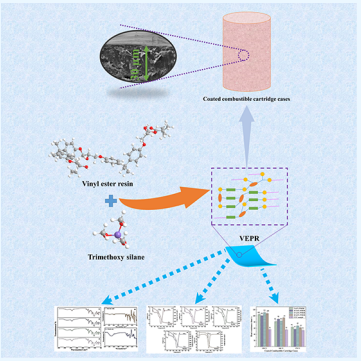

1. INTRODUCTION

Combustible cartridge cases (CCCs) with nitrocellulose-containing walls offer advantages such as eliminating spent cases in closed crew compartments, increasing firing rates, and simultaneously reducing reloading times. The overall logistic burden on the support system is thus reduced, resulting in an improvement in the ballistics efficiency of the round that is widely utilized in high-caliber tank gun ammunition around the globe.[1−3] However, CCCs with nitrocellulose as an energetic component are considered unsafe due to their high sensitivity to friction, heat, and static electricity.[4−6] Additionally, during long-term storage and transportation, CCCs tend to absorb moisture and corrosive gases due to their superficial porous structure, resulting in reduced instantaneous combustion rates and incomplete combustion.[7,8] It is therefore imperative to implement effective measures to improve the thermal stability, water resistance, and resistance to salt corrosion of CCCs.

One approach for improving the overall performance of CCCs is the use of composite protective coating. Zhang et al.[9] have developed a composite coating capable of withstanding a temperature of 220 °C for 138 s, with a final water absorption of 0.2944% upon immersing in highly saline water at 26 °C for 3 days, demonstrating an effective improvement in the heat and salt resistance of CCCs. Chen et al.[10] utilized fluorine-containing nanocomposite material and nitrocellulose as film-forming materials to prepare a multifunctional composite coating on the surface of CCCs, which led to improved mechanical properties and environmental adaptability. Furthermore, Zhang et al.[11] designed a new composite surface coating for CCCs that resisted burning at 230 °C for 108.8 s. The coating significantly enhanced the ability of CCCs to withstand high temperatures and resist water, achieving a water contact angle of 105.71°. Consequently, composite coatings present a promising solution to protect CCCs as well as improve their performance. Until now, several studies have been carried on the preparation and modification of protective coatings for CCCs. However, there is limited research on enhancing the heat resistance and thermal stability of CCC protective coatings.

Vinyl ester (VE)-based composite resins have been extensively used to build structural parts in various industries including automobiles, marine construction, storage tank fabrication, pipeline manufacturing, and residential development.[12] VE resins are often used in the production of fiber-reinforced plastics because of their inherent advantages, such as affordability, thermal stability, ease of processing, good mechanical strength, and corrosion resistance.[13,14] However, VE resins are more flammable than epoxy resins and cause dense smoke upon ignition.[15,16] This property renders the composite materials prepared with VE resins inadequate to meet the high fire safety requirements in certain applications, including transportation, aerospace, and infrastructure sectors.

Phenolic resin, known for its exceptional thermal stability, flame retardancy, and mechanical strength, has been

Received: July 10, 2024
Revised: March 8, 2025
Accepted: March 11, 2025
Published: April 1, 2025

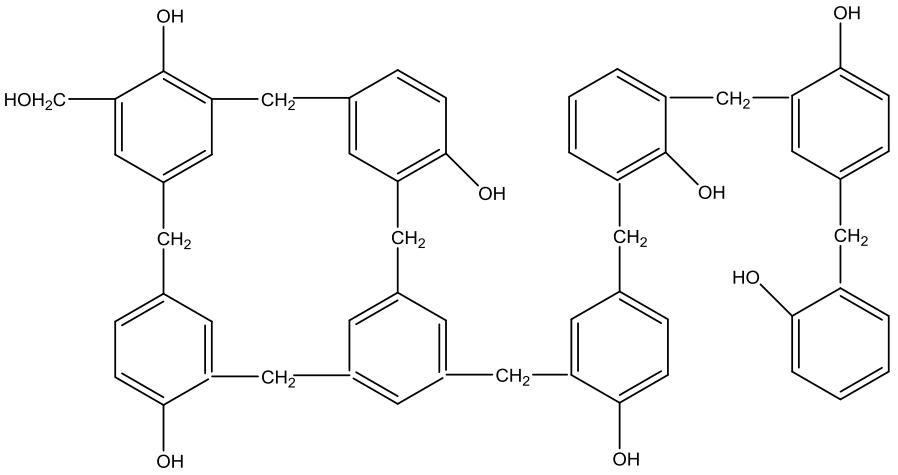

Figure 1. Chemical structure of phenolic resin.

extensively utilized in flame retardant materials, grinding wheel manufacturing, ablative thermal protection systems, and molding compounds.[17] Guo et al.[18] have proposed that the methylene and phenolic hydroxyl groups in phenolic resin are susceptible to oxidation, reducing its chemical reactivity and seriously limiting its potential applications in other areas. Numerous strategies have been implemented to improve the oxidation resistance of phenolic resin. Balandin et al.[19] and Zhao et al.[20] have demonstrated that incorporating graphene in phenolic resin significantly enhances its thermal stability due to the single-layered two-dimensional structure of graphene. Alternative approaches, including the incorporation of antioxidants such as boron, silicon, titanium, and phosphorus into the backbone of phenolic resins, were also reported.[21−25] Research into modified phenolic resins is continuing to meet the demands across diverse fields.

Herein, we prepared a novel resin composite coating as a film-forming material. In addition to the hybridization of vinyl ester (VE) resin and phenolic resin, the incorporation of an epoxy-amine curing system plays a critical role in forming a robust cross-linked network. This synergistic interaction contributes significantly to the coating's high thermal stability, hydrophobicity, and heat resistance, as demonstrated in this study. The microstructure and the thermal and corrosion-resistant properties of the coatings were comprehensively investigated. Especially the heat resistance time of coated CCCs was tested at 250 °C, 260 °C, and 270 °C. The synthesis and protective performance correlations of the novel vinyl ester-modified phenolic resin (VEPR) composite coating presented in this work thereby provide fundamental implications for the future design of advanced protective coatings for CCCs.

2. MATERIALS AND METHODS

2.1. Materials. The resin tested in the present study was the two-component VE resin (AR) ATLAC 580 ACT supplied by DSM Composite Resins (France S.A.). Figure 1 shows its chemical structure. The VE monomer containing two vinyl end groups allows cross-linking during the reaction. Methyl ethyl ketone peroxide (MEKP, AR) was supplied by Huntsman Chemical Company, Australia. The supplier of the 30 nm yttria-stabilized zirconia was Shanghai Yaoyi Alloy Material Co., Ltd., China. We bought the epoxy resin curing agent 593 (GR, 99.0%) and benzyl glycidyl ether (GR, 99.0%) from Suzhou Qicai Stone Composite Material Co., Ltd. in China. The supplier of nanosilica (20 nm) was Shanghai Meiruil Chemical Technology Co., Ltd., China. Glass bubbles K1 (density 0.125 g cm^{-3}, PSI 250, D50 Micron 65, strength 1.7 MPa, 180 mesh) were provided by Sinopharm Group, China.

Silane coupling agent (KH550, CP) was provided by Shanghai Yaoyi Alloy Material Co., Ltd., China. The emulsifiers OP-4 (octaphenyl polyoxyethyiene, AR) and Tween 80 (AR) were provided by Nanjing Middle East Glass Instrument Co., Ltd., China. Karstedt's catalyst, supplied by Macklin, China, is a complex solution containing Pt_2(1,3-divinyl-1,1,3,3-tetramethyldisiloxane)$_3$ in xylene with a platinum metal content of approximately 2%. The phenolic resin was purchased from Aladdin, China. Figure 1 shows the chemical structure of the phenolic resin.

2.2. Synthesis of Phenolic Resin-Modified Vinyl Ester Resin. For the silane modification, vinyl ester (VE) resin (100 g) was reacted with trimethoxysilane (2.5 g) in the presence of Karstedt's catalyst (0.2 mL, 2% platinum content in xylene) under stirring at 60 °C for 30 min (shown in Figure 2). The weight ratio of VE resin to trimethoxysilane was maintained at 40:1.

The phenolic resin was added to the silane-modified VE resin in a weight ratio of 1:5 (phenolic resin: total resin mixture). This ratio was optimized based on preliminary testing to achieve the desired balance of thermal stability and mechanical properties. Then, OP-4 emulsifier and Tween 80 were added to the mixture, followed by stirring for 1 h at 50

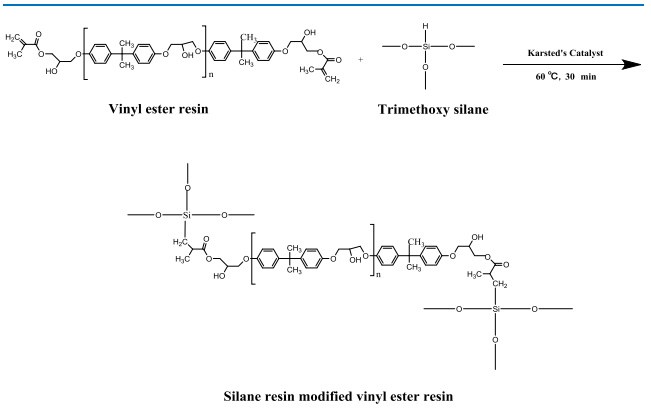

Figure 2. Synthesis of silane-modified VE resin.

https://doi.org/10.1021/acsomega.4c06375
ACS Omega 2025, 10, 13807−13815

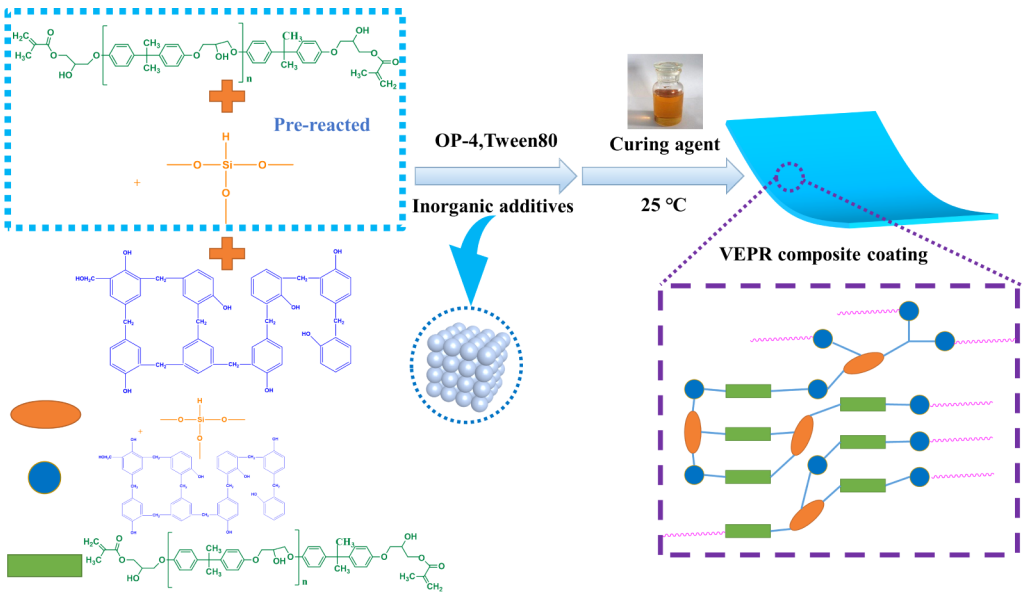

Figure 3. Fabrication route of VEPR composite mixture.

Table 1. Formula of VEPR Composite Coating

Formulation	VEPR (g)	Phenolic Resin (g)	OP-4 Emulsifier (g)	Tween 80 (g)	Glass Bubbles K1 (g)	Nano-Silica (g)	Yttria-Stabilized Zirconia (g)	MEKP (g)	Curing Agent 593 (g)	Benzyl Glycidyl Ether (g)
5 wt % VEPR	1.1	0.22	2.0	2.0	3.0	3.0	2.0	4.0	5.0	4.3
10 wt % VEPR	2.3	0.46	2.0	2.0	3.0	3.0	2.0	4.0	5.0	4.3
15 wt % VEPR	3.7	0.74	2.0	2.0	3.0	3.0	2.0	4.0	5.0	4.3
20 wt % VEPR	5.3	1.06	2.0	2.0	3.0	3.0	2.0	4.0	5.0	4.3

Table 2. Control Experiment Design and Results

Sample Type	Thermal Stability (T5%, °C)	Water Contact Angle (°)	Heat Resistance Time at 250 °C (s)	Observation
Silane-modified VE resin without phenolic	175.3	95.8	90	Improved performance over pure VE resin, suggesting silane contributes to stability and hydrophobicity.
Hybrid VE/phenolic without silane	185.2	88.4	95	Moderate improvement compared to pure phenolic, indicating phenolic-VEs provide inherent benefits.
VE with increased silane concentration	180.1	100.2	92	Benefits observed due to increased silane content, but still lower than the hybrid VE/phenolic structure.
Hybrid VE/phenolic without epoxy-amine	182.3	90.5	96	Performance lower than complete hybrid system, indicating a synergistic role of the epoxy-amine curing component.

°C. This combination was supplemented with glass bubbles K1 and nanosilica to increase the heat resistance of the VEPR mixture. The yttria-stabilized zirconia was ground using a ball mill for 30 min before adding to the above mixture. Then, the benzyl glycidyl ether was added into the mixture and agitated for 20 min at 60 °C. Finally, a homogeneous solution mixture was obtained. The entire fabrication routine of the VEPR composite mixture is presented in Figure 3.

2.3. Preparation of VEPR Composite Coating. MEKP and the epoxy resin curing agent 593 were mixed at a 1:2 weight feed ratio and stirred for 10 min to prepare a novel curing agent. The curing agent was then added to the VEPR composite mixture, followed by stirring at 25 °C for 15 min to yield the VE resin composite mixtures. Finally, based on the silane-modified VE resin content, four mixtures with 5, 10, 15, and 20 wt % VEPR composite coatings were prepared. The formula details of VEPR composite coatings is listed in Table 1.

2.4. The Coating Process of Combustible Cartridge Cases. The curing agent was prepared by mixing MEKP and epoxy curing agent 593 in a 4:5 weight ratio. The curing agent was then added to the VEPR composite mixture and stirred for 15 min at 25 °C to yield the VE resin composite mixtures. A high-precision analytical balance was used to measure the starting weights of each component in accordance with recognized methods.[26,27] Next, to guarantee complete mixing, the mixture was swirled for 3−5 min. On the CCC surfaces, the slurry was uniformly sprayed using an electric sprayer (SG0140-EU650). The CCC samples measured 30.0 cm by 10.0 cm by 0.25 cm. The coated samples were sprayed and then placed into the air atmosphere and set the heat temperature at 25 °C for 12 h to obtain coated CCCs.

https://doi.org/10.1021/acsomega.4c06375
ACS Omega 2025, 10, 13807−13815

Table 3. Cure Mechanisms Analysis

Cure Mechanism	Evidence	Contribution to Coating
Silane Condensation	Observed through FTIR peaks at ~1025 cm^{-1} (Si−O−Si bonds) and ~2850 cm^{-1} (Si-CH3)	Enhances cross-linking density and hydrophobicity, improves resistance to environmental factors
Phenol Condensation	Confirmed by FTIR peaks at ~1600 cm^{-1} (C═C in phenolic ring) and ~3200 cm^{-1} (OH group reduction)	Contributes to thermal stability and mechanical strength
Phenol-Epoxy Reaction	Indicated by the appearance of peaks at ~1250 cm^{-1} (C−O−C bonds) and ~1710 cm^{-1} (ester groups)	Provides strong adhesion and additional cross-linking
Epoxy-Amine Reaction	Observed through FTIR signals at ~3400 cm^{-1} (NH stretching) and TGA analysis	Improves thermal resistance of the coating
Peroxide-Initiated	TGA analysis shows mass loss at 200−250 °C, corresponding to the decomposition of peroxide initiators	Triggers polymerization of the vinyl ester, contributing to the initial network formation

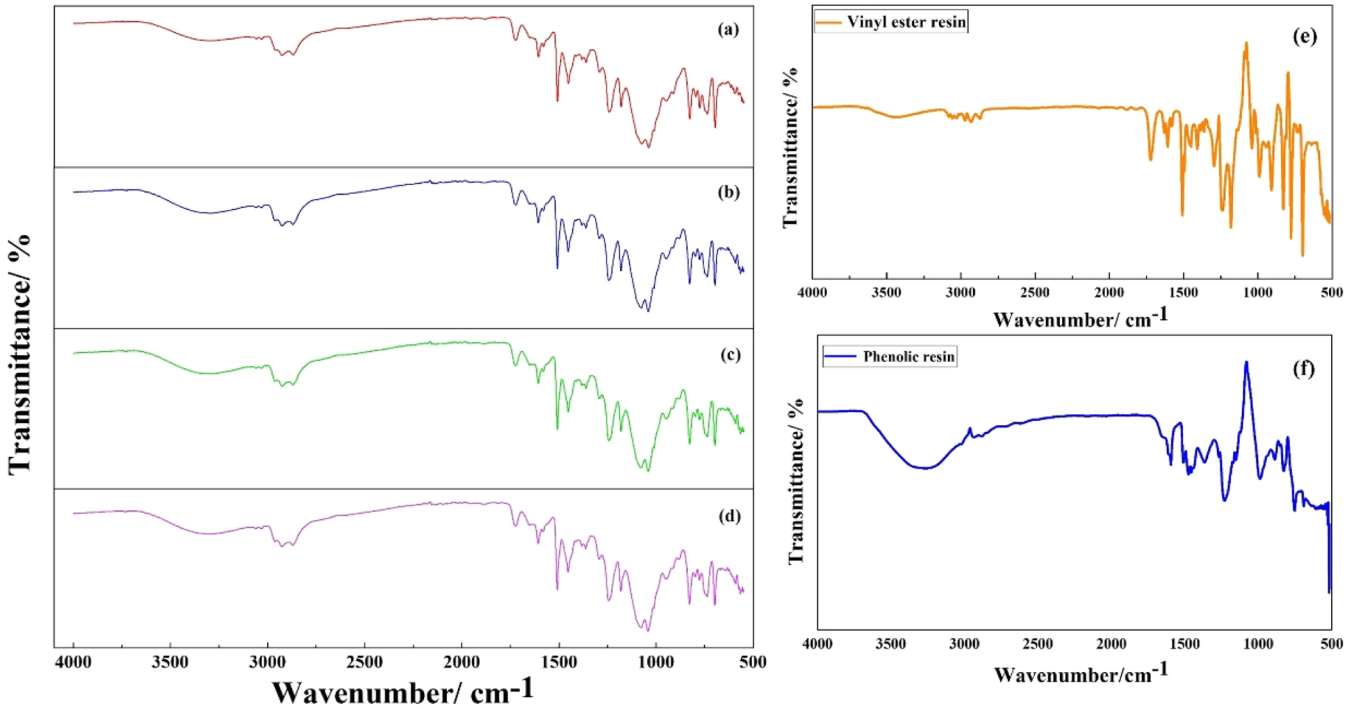

Figure 4. FTIR spectra of VEPR composite coatings. (a) 5 wt % VEPR, (b) 10 wt % VEPR, (c) 15 wt % VEPR, (d) 20 wt % VEPR, (e) vinyl ester resin, and (f) phenolic resin.

Moreover, the thickness of coated CCC specimens was controlled at 30.0 μm ± 5.0 μm by mold.

The chemical structures of the VEPR composite coatings were analyzed by FTIR spectroscopy. To comprehensively investigate the thermal stability and heat resistance of VEPR, TGA, DSC, and heat resistance tests were performed. Furthermore, the micromorphology and the elemental distribution on the surface of coated CCC samples were obtained by SEM-EDS and XPS.

3. CONTROL EXPERIMENT AND CURE MECHANISMS

Through the follow experimental results (seen in Tables 2 and 3), we have successfully revealed the curing mechanism of VEPR composite coatings, forming a multilayered chemical network that imparts superior thermal stability and mechanical performance to the coating. Meanwhile, we have concluded control experiment and cure mechanisms which was listed in Supporting Information (Tables S1 and S2), providing a solid theoretical basis for the final performance of the composite coatings.

The curing mechanism of the VEPR coatings involves several key chemical reactions that form a dense, multilayered cross-linked network, which is responsible for the superior thermal, hydrophobic, and mechanical properties of the coatings.

These chemical mechanisms are strongly supported by the experimental data. The TGA results demonstrate the superior thermal stability imparted by this curing mechanism, with the 15 wt % VEPR coating showing a T5% of 199.2 °C compared to 165.2 °C for pure VE resin. Water contact angle measurements align with the hydrophobicity enhancement from silane modification, with the 20 wt % VEPR coating achieving the highest WCA of 112.5°, significantly improving moisture resistance. Furthermore, the heat resistance time at 250 °C for the 15 wt % VEPR coating reached 111 s, showcasing its ability to delay heat penetration due to the multilayered cross-linked network. These experimental results directly validate the curing mechanism and highlight the synergistic effects of silane-modified vinyl ester resin, phenolic resin, and the epoxy-amine curing system. Presenting the curing mechanism first allows the experimental findings to be understood as direct evidence supporting the proposed chemical interactions.

https://doi.org/10.1021/acsomega.4c06375
ACS Omega 2025, 10, 13807−13815

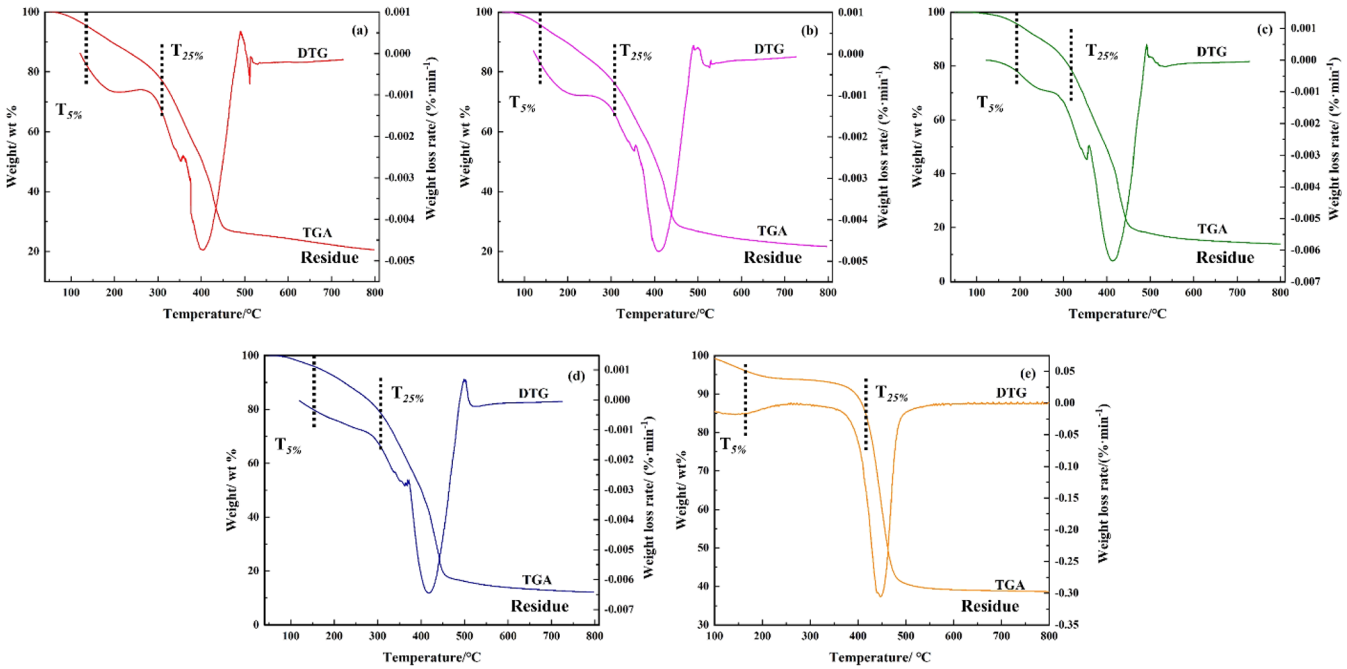

Figure 5. Thermogravimetric curves of VEPR composite coatings. (a) 5 wt % VEPR, (b) 10 wt % VEPR, (c) 15 wt % VEPR, (d) 20 wt % VEPR, and (e) VE.

4. RESULTS AND DISCUSSION

4.1. Spectral Analysis. Figure 4 shows the FTIR spectra of the various VEPR composite coatings. C═C vibrations are responsible for the peaks observed between 1600 and 1450 cm^{-1}.[28−30] The C−O vibrations of methylol aromatic groups and aliphatic groups cause the signals with absorption maxima at around 1015 and 1250 cm^{-1}, respectively.[31,32] The FTIR spectra of the VEPR coatings exhibit characteristic peaks in the range of 2800−3000 cm^{-1}, which correspond to CH stretching vibrations from CH_3 and CH_2 groups.[33,35] Additional peaks, such as the ester carboxyl group vibration at 1713 cm^{-1} and the C−O vibrations at 1015 and 1250 cm^{-1}.[34] The first step is silane condensation, where Si−O−Si bonds are formed through the reaction of trimethoxysilane with vinyl ester resin, as confirmed by the FTIR peak at ∼1025 cm^{-1}. This reaction enhances the cross-linking density and hydrophobicity of the coating. The second reaction is phenol condensation, where hydroxyl groups in the phenolic resin undergo condensation reactions, as indicated by the FTIR reduction in OH group peaks at ∼3200 cm^{-1} and the presence of C═C stretching peaks at ∼1600 cm^{-1}. This reaction contributes to the thermal stability and mechanical strength of the coating. Additionally, the phenol-epoxy reaction results in the formation of C−O−C bonds (∼1250 cm^{-1} in FTIR), which further strengthens the network. Finally, epoxy-amine polymerization, confirmed by NH stretching peaks at ∼3400 cm^{-1}, adds structural integrity and improves thermal resistance.

4.2. Thermal Analysis. Using TGA in a nitrogen environment, the thermal degradation behaviors of the VEPR composite coatings were examined. Figure 5 presents the TGA curves. According to Figure 5a−d, all samples exhibited a consistent trend of a two-step degradation pattern. The slight mass loss in the range of 200−300 °C was caused by the evaporation of the OP-4 emulsifier (boiling point of 250 °C) and the partial decomposition of VEPR. A subsequent sharp drop occurred between 350 and 500 °C, which was attributed to the thermal decomposition of VEPR. Referring to Table 4, this sharp drop was observed at different temperatures depending on the phenolic resin content of the VEPR samples. The thermal degradation of pure VE resin exhibited a cumulative mass loss of 25% at 395.0 °C and 75% at 438.0 °C. Furthermore, it was observed that the T_g temperatures of modified VEPR samples were higher than those of pure VE resin. Notably, the 15 wt % VEPR composite coating exhibited the highest $T_{5\%}$ of 199.2 °C. Thus, the 15 wt % VEPR sample demonstrated optimum thermal stability among the materials. Combined with Figures 7 and 8(II), the above results indicate that the dense surface structure could contribute to its thermal stability.

Table 4. Thermogravimetric Analysis Results of VEPR Composite Coatings

Test Name	Thermogravimetric Analysis Nitrogen	
Sample Name	$T_{5\%}$ (°C)	$T_{25\%}$ (°C)
5 wt % VEPR	140.3 ± 2.6	319.2 ± 2.5
10 wt % VEPR	143.7 ± 2.6	314.1 ± 2.7
15 wt % VEPR	199.2 ± 2.4	329.9 ± 1.9
20 wt % VEPR	167.4 ± 2.2	322.5 ± 2.1
VE	165.2 ± 1.8	432.1 ± 2.1

The control experiment "hybrid VE/phenolic without epoxy-amine" exhibited reduced thermal stability ($T_{5\%}$: 182.3 °C) and heat resistance time (96 s at 250 °C) compared to the complete hybrid system ($T_{5\%}$: 199.2 °C; 111 s at 250 °C). This result confirms that the epoxy-amine curing system contributes to the high-performance characteristics of the coating by enhancing the cross-linking density, thermal stability, and structural integrity.

While the 15 wt % VEPR coating demonstrated the highest average heat resistance time at 250 °C (111 s), the values for all four VEPR samples overlap within the error bars. Therefore, it cannot be stated with statistical confidence that the 15 wt %

https://doi.org/10.1021/acsomega.4c06375
ACS Omega 2025, 10, 13807−13815

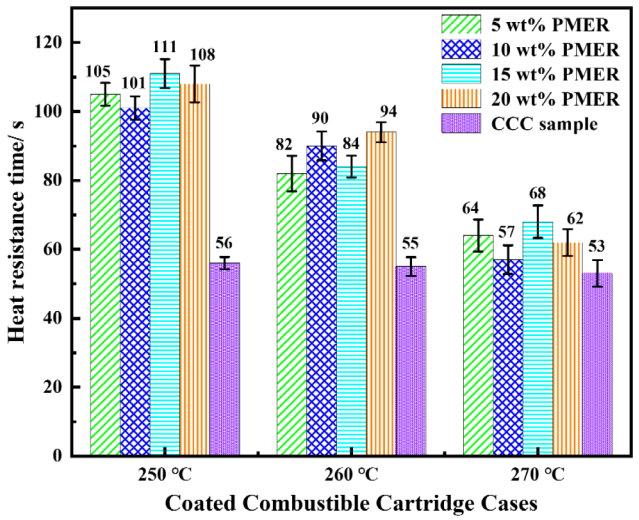

Figure 6. Average heat resistance time of coated combustible cartridge case samples.

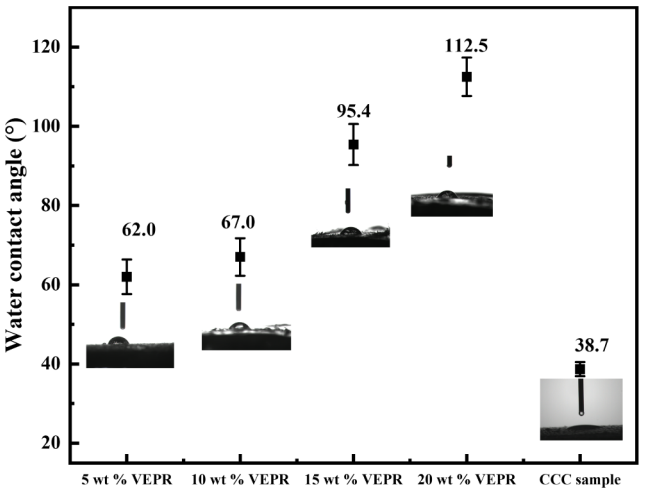

Figure 8. Water contact angle of the exterior surface of combustible cartridge case samples coated with VEPR composite.

Table 5. EDS Analysis of the Surface Element Content of VEPR Composite Coatings

	C (wt %)	N (wt %)	O (wt %)	Si (wt %)
5 wt % VEPR	53.3	3.8	42.7	0.3
10 wt % VEPR	65.4	7.3	26.5	0.8
15 wt % VEPR	63.0	5.7	28.9	2.5
20 wt % VEPR	64.9	7.7	25.2	2.1

VEPR coating performed significantly better than the other formulations without additional rigorous statistical analysis (e.g., *t* test). Nonetheless, the trend suggests that the 15 wt % VEPR coating offers optimal thermal protection under the tested conditions, likely due to its balanced composition of silane-modified VE resin, phenolic resin, and inorganic fillers.

4.3. Surface Compositional Analysis. The chemical composition of the VEPR composite coating was analyzed by EDS. The spectra shown in Supporting Information reveal the presence of carbon, oxygen, silicon, and nitrogen on the surfaces of the VEPR composite coatings. Table 5 lists the percentages of these elements in all the VEPR samples. The images showed an abundance of carbon and oxygen with lower contents of nitrogen and silicon in agreement with the XPS results (seen in Supporting Information). The small content of silicon could have combined with oxygen, carbon, and nitrogen to form Si−O−Si, Si−C, and Si−N moieties, attributed to VEPR.[36,37] Consequently, the existence of these silicon bonds could improve the thermal stability and hydrophobicity of the VEPR composite coatings.

XPS analysis revealed the existence of carbon, oxygen, nitrogen, and silicon in different forms. From Figures S2−S5, C 1s XPS spectra revealed the presence of C−O single bonds (286.7 eV) and C = O double bonds (283.6 eV).[38−40] Furthermore, the O 1s XPS spectra (Figures S6−S9) exhibited

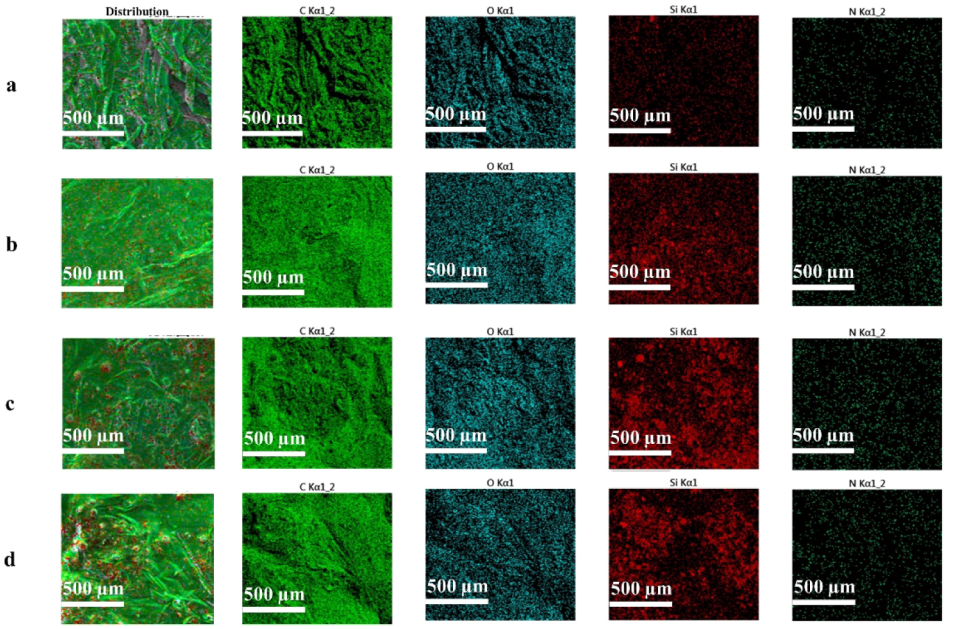

Figure 7. EDS elemental mappings of VEPR composite coatings. (a) 5 wt % VEPR, (b) 10 wt % VEPR, (c) 15 wt % VEPR, and (d) 20 wt % VEPR.

https://doi.org/10.1021/acsomega.4c06375
ACS Omega 2025, 10, 13807−13815

a broad peak at 531.2 eV, which was caused by C−O bonds.[41,42]

4.4. Water Resistance Analysis. Figure 8 shows the WCAs of the exterior surfaces of the various VEPR composite coatings. Generally, phenolic resins and CCCs are hydrophilic due to their inherent hydrophilic groups, such as methoxy and hydroxyl. However, the VEPR composite coating in this study exhibited excellent hydrophobic properties. It was observed that the WCA of the coated CCC samples improved with the increase in silane-modified VE resin content. Consequently, the WCA of the CCC sample coated with 20 wt % VEPR reached the highest value of 112.5°. Furthermore, the CCC sample with 15 wt % VEPR coating exhibited significant waterproofing properties. This improvement effectively prevented moisture from entering the interior of the CCC, thereby enhancing environmental adaptability.

As shown in Figure 9, cracks developed on the surfaces of the CCC samples when subjecting them to a salt-spray test.

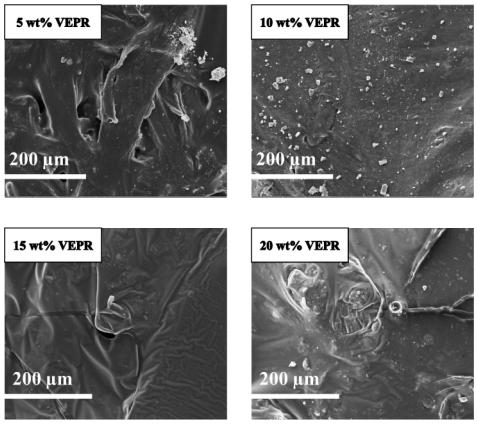

Figure 9. SEM micrographs of combustible cartridge case samples coated with VEPR composite after 3 days of exposure to a high-salt wet experimental environment.

The 5 wt % VEPR composite coating was seriously damaged, exposing the entire CCC surface while no coating-covered area remained, thus providing the poorest protection. By contrast, the cracks observed for the 15 wt % VEPR composite coating sample were the smallest compared to those developed in other samples, suggesting its optimum resistance to salt corrosion. The reason was attributed to the cross-linking role of VEPR. The findings of the study on the damaged surface morphologies were consistent with the results of the heat resistance tests (Figure 6), demonstrating the superior protective effect of 15 wt % VEPR composite coating on CCCs. After 3 days of exposure to the high-salt wet environment, a white solid was observed on the exterior surface of all coated samples. This white solid was confirmed to be salt deposits formed as a result of the salt spray test. These deposits indicate the effective prevention of salt and moisture penetration into the combustible cartridge cases (CCCs) by the VEPR composite coatings.

To further elucidate the final coating structure, a series of comprehensive analytical techniques were employed. First, Fourier Transform Infrared Spectroscopy (FTIR) provided detailed insights into the bonding within the coating, confirming the presence of functional groups such as Si−O−Si, C−O−C, NH, and phenolic C═C bonds, all of which indicate the chemical reactions occurring during the curing process. Next, X-ray Photoelectron Spectroscopy (XPS) revealed the elemental composition of the coating surface, further confirming the successful silane and phenolic cross-linking. Notably, the identification of Si−O−Si bonds validated the formation of a silane-based chemical network at the surface layer. Finally, Thermal Analysis (DSC and TGA) was instrumental in identifying key thermal transitions and decomposition patterns, allowing us to determine the temperature ranges required for each curing mechanism to proceed effectively.

Based on the experimental results, we propose the following multistep curing mechanism: First, silane condensation (50−80 °C) begins at lower temperatures, forming Si−O−Si cross-links that lay the foundation of the coating structure. As the temperature rises, the epoxy-amine reaction (100−120 °C) starts, contributing to the network formation and enhancing the structural stability of the coating. At higher temperatures (150−200 °C), phenol condensation and phenol-epoxy reactions take place, significantly improving the thermal stability and structural integrity. Finally, peroxide-initiated polymerization concurrently drives vinyl ester cross-linking, completing the hybrid network and further enhancing the mechanical properties and environmental stress resistance of the coating.

4.5. Performance Comparison and Analysis. Table 6 provides a comparison of the thermal stability, water resistance, and heat resistance time of the VEPR composite coatings with pure vinyl ester (VE) and phenolic resin. The 15 wt % VEPR composite coating showed a substantial improvement in all properties compared to the control systems. Its thermal stability was significantly higher than that of pure VE, with a T5% of 199.2 °C, and it exhibited a superior water contact angle (95.4°), reflecting its enhanced hydrophobicity. Most notably, the heat resistance time at 250 °C for the 15 wt % VEPR-coated sample was 111 s, the longest among all the samples, demonstrating its optimal performance in preventing heat penetration. These results suggest that the 15 wt % VEPR composite coating offers an excellent balance of thermal stability, water resistance, and heat resistance, making it a promising candidate for protective applications.

5. CONCLUSION

In this study, four VEPR composite coatings with different phenolic resin content were successfully synthesized. According to the results of the WCA tests, there was an increasing trend in the hydrophobicity of the VEPR composite coatings

Table 6. Comparison Performance of the Hybrid VE/Phenolic System with Control Systems

Type	Thermal Stability (T5%, °C)	Thermal Stability (T25%, °C)	Water Contact Angle (°)	Heat Resistance Time at 250 °C (s)
Pure Vinyl Ester (VE)	165.2 ± 1.8	432.1 ± 2.1	78.6 ± 4.8	79.0 ± 3.5
Pure Phenolic Resin	110.5 ± 2.2	351.1 ± 1.9	37.6 ± 4.4	69.5 ± 4.0
Hybrid VE/Phenolic (15 wt %)	199.2 ± 2.4	329.9 ± 1.9	95.4 ± 5.2	111 ± 4.2

https://doi.org/10.1021/acsomega.4c06375
ACS Omega 2025, 10, 13807−13815

with the increase in phenolic resin content. The XPS results proved the existence of silicon oxide on the surface as suggested by the presence of a very broad peak at 102.5 eV in the Si 2p XPS spectrum corresponding to Si−O−Si, which effectively enhanced the hydrophobicity of VEPR composite coating. According to Table 4, all coated CCC samples possessed excellent heat resistance. Among them, the 15 wt % VEPR-coated CCC sample exhibited the longest heat resistance time of 111 s at 250 °C, indicating optimal performance in preventing heat from penetrating the CCC. The high performance of the VEPR composite coatings is attributed to the synergistic effects of the hybrid vinyl ester, phenolic resin, and epoxy-amine curing system. This combination forms a multilayered chemical network that imparts superior thermal stability, hydrophobicity, and heat resistance, making it an optimal formulation for CCC protection.

■ ASSOCIATED CONTENT

Data Availability Statement

Due to laboratory privacy restrictions and related ethical considerations, the research data underlying this study cannot be made publicly available.

Supporting Information

The Supporting Information is available free of charge at https://pubs.acs.org/doi/10.1021/acsomega.4c06375.

Detailed description of control coating preparation; characterization; water contact angle test; salt resistance test; heat resistance test; XPS results (PDF)

■ AUTHOR INFORMATION

Corresponding Author

Zhenggang Xiao − *Key Laboratory of Special Energy Materials, Ministry of Education, School of Chemistry and Chemical Engineering, Nanjing University of Science and Technology, Nanjing 210094, China;* orcid.org/0000-0002-7836-1397; Email: xiaozhg@njust.edu.cn

Author

Mengde Wu − *Key Laboratory of Special Energy Materials, Ministry of Education, School of Chemistry and Chemical Engineering, Nanjing University of Science and Technology, Nanjing 210094, China*

Complete contact information is available at: https://pubs.acs.org/10.1021/acsomega.4c06375

Author Contributions

M.W.: conceptualization, formal analysis, writing—original draft. Z.X.: funding acquisition.

Funding

This work was partly supported by the National Natural Science Foundation of China (No. 22075146). We thank the Postgraduate Research Practice Innovation Program of Jiangsu Province (No. KYCX23_0449) for supporting this work.

Notes

The authors declare no competing financial interest.

Reproducibility statement: All the experimental data in this paper can be obtained by repeated experiments.

■ ACKNOWLEDGMENTS

I would like to extend my sincere gratitude to Professor Xiaoheng Liu and Pingyun Li for their advice and useful suggestions on my writing. We would like to thank MogoEdit (https://www.mogoedit.com) for its English editing during the preparation of this manuscript.

■ REFERENCES

(1) Kurulkar, G. R.; Syal, R. K.; Singh, H. Haridwar Singh, Combustible cartridge case formulation and evaluation. *J. Energ. Mater.* **1996**, *14* (2), 127−149.

(2) Miguel, S. A. Design criteria for inert or consumable polymer cartridge materials. *J. Spacecr. Rockets* **1973**, *10* (5), 333−340.

(3) Ho, C. -H.; Tomkins, B. A.; Ramsey, R. S.; Griest, W. H.; Counts, R. W. Determination of nitroester and stabilizer migration in combustible cartridge case wall. *Propellants, Explos., Pyrotech.* **1996**, *21* (2), 79−84.

(4) Nagayama, K.; Oyumi, Y. Combustion characteristics of high burn rate azide polymer propellant. *Propellants, Explos., Pyrotech.* **1996**, *21* (2), 74−78.

(5) Wu, M.; Xiao, Z. Optimum preparation of organopolysilazane composite coatings and their role in protecting combustible cartridge cases. *Surf. Interfaces* **2025**, *58*, 105804.

(6) Wu, M.; Cao, G.; Xiao, Z. Polyimide-modified epoxy coatings reinforced with functional fillers for enhanced thermal stability and corrosion resistance. *Adv. Compos. Hybrid Mater.* **2025**, *8*, 172.

(7) Wu, M.; Xiao, Z. Enhancement of heat resistance and waterproof performance of combustible cartridge cases with phenolic epoxy resin-modified polydimethylsiloxane composite coating. *Colloids Surf., A* **2025**, *708*, 136002.

(8) Jehličková, E.; Zubek, V.; Konečný, P.; Kubát, K. Combustible cartridge case material characteristics evaluation. *Propellants, Explos., Pyrotech.* **2024**, *49* (9), No. e202400100.

(9) Zhang, Y.; Zeng, X.; Xiao, J.; Pu, C.; Shi, H.; Xiao, Z. Preparation and properties of coating for improving heat and salt wet resistance of combustible cartridges. *Propellants, Explos., Pyrotech.* **2020**, *45*, 1149−1155.

(10) Chen, S.; Shi, H.; Tian, S.; Li, Z.; Xiao, Z. Design and fabrication of a composite coating to improve the environmental adaptability of combustible cartridges. *Polym. Compos.* **2019**, *40* (2), 685−694.

(11) Zhang, B.; Fu, E.; Shi, H.; Zhang, X.; Xiao, Z. Improvement in high temperature-resistant performance and waterproof property of combustible cartridge case with BEMS resin based composite coating. *Propellants, Explos., Pyrotech.* **2022**, *47* (3), 202100303.

(12) Murillo, E. A. Waterborne star-shaped styrene-alkyd resins. *J. Appl. Polym. Sci.* **2020**, *137* (8), 48386.

(13) Yang, R.; Wang, Y.; Ran, X.; Liu, W. A Comparison Study on Toughening Vinyl Ester Resins Using Different Nanocarbon Materials. *Polymers* **2023**, *15* (23), 4536.

(14) Sultania, M.; Yadaw, S. B.; Rai, J. S. P.; Srivastava, D. Laminates based on vinyl ester resin and glass fabric: A study on the thermal, mechanical and morphological characteristics. *Mater. Sci. Eng., A* **2010**, *527*, 4560−4570.

(15) Kandola, B. K.; Ebdon, J. R.; Zhou, C. Development of vinyl ester resins with improved flame retardant properties for structural marine applications. *React. Funct. Polym.* **2018**, *129*, 111−122.

(16) Prabhakar, M.; Song, J. Influence of chitosan-centered additives on flammable properties of vinyl ester matrix composites. *Cellulose* **2020**, *27* (14), 8087−8103.

(17) Hirano, K.; Asami, M. Phenolic resins—100years of progress and their future. *React. Funct. Polym.* **2013**, *73* (2), 256−269.

(18) Guo, Y.; Hu, L.; Jia, P.; Zhang, B.; Zhou, Y. Enhancement of thermal stability and chemical reactivity of phenolic resin ameliorated by nanoSiO_2. *Korean J. Chem. Eng.* **2018**, *35* (1), 298−302.

(19) Balandin, A. A.; Ghosh, S.; Bao, W.; Calizo, I.; Teweldebrhan, D.; Miao, F.; Lau, C. N. Superior thermal conductivity of single-layer graphene. *Nano Lett.* **2008**, *8* (3), 902−907.

(20) Zhao, Y.; Wu, Z.; Bai, S. Study on thermal properties of graphene foam/graphene sheets filled polymer composites. *Compos., Part A* **2015**, *72*, 200−206.
(21) Chai, Y.; Liu, J.; Zhao, Y.; Yan, N. Characterization of modified phenol formaldehyde resole resins synthesized in situ with various boron compounds. *Ind. Eng. Chem. Res.* **2016**, *55* (37), 9840−9850.
(22) Li, S.; Han, Y.; Chen, F.; Luo, Z.; Li, H.; Zhao, T. The effect of structure on thermal stability and antioxidation mechanism of silicone modified phenolic resin. *Polym. Degrad. Stab.* **2016**, *124*, 68−76.
(23) Li, C.; Ma, Z.; Zhang, X.; Fan, H.; Wan, J. Silicone-modified phenolic resin: Relationships between molecular structure and curing behavior. *Thermochim. Acta* **2016**, *639*, 53−65.
(24) Qiao, W.; Li, S.; Xu, F. Preparation and characterization of a phenol-formaldehyde resin adhesive obtained from bio-ethanol production residue. *Polym. Polym. Compos.* **2016**, *24* (2), 99−105.
(25) Zhang, Y.; Shen, S.; Liu, Y. The effect of titanium incorporation on the thermal stability of phenol-formaldehyde resin and its carbonization microstructure. *Polym. Degrad. Stab.* **2013**, *98* (2), 514−518.
(26) Xing, C.; Yi, M.; Shan, X.; Wang, X.; Zhao, X.; Guo, F. Sintering behavior of a nanostructured thermal barrier coating deposited using electro-sprayed particles. *J. Am. Ceram. Soc.* **2020**, *103* (12), 7267−7282.
(27) Canak, T. C.; Ünsal, C.; Serhatlı, I. E.; Sarac, A. S. Superhydrophobic fluorinated acylonitrile coatings via electrospraying. *Prog. Org. Coat.* **2017**, *105*, 342−352.
(28) Chen, M.; Hu, W.; Liang, X.; Zou, C.; Li, F.; Zhang, L.; Chen, F.; Yang, H. A facile all-solution-processed surface with high water contact angle and high water adhesive force. *ACS Appl. Mater. Interfaces* **2017**, *9* (27), 23246−23254.
(29) Tu, L.; Xiao, Q.; Wei, R.; Liu, X. Fabrication and enhanced thermal conductivity of boron nitride and polyarylene ether nitrile hybrids. *Polymers* **2019**, *11* (8), 1340.
(30) Tang, K.; Lv, X.; Wu, S.; Xuan, S.; Huang, X.; Bai, C. Measurement for contact angle of iron ore particles and water. *ISIJ Int.* **2018**, *58* (3), 379−400.
(31) Caddeo, C.; Marongiu, D.; Meloni, S.; Filippetti, A.; Quochi, F.; Saba, M.; Mattoni, A. Hydrophilicity and water contact angle on methylammonium lead iodide. *Adv. Mater. Interfaces* **2019**, *6*, 1801173.
(32) Wang, D.; Ding, J.; Wang, B.; Zhuang, Y.; Huang, Z. Synthesis and thermal degradation study of polyhedral oligomeric silsesquioxane (POSS) modified pf resin. *Polymers* **2021**, *13*, 1182.
(33) Hassan, R. M. Novel synthesis of natural cation exchange resin by crosslinking the sodium alginate as a natural polymer with 1,6-hexamethylene diisocyanate in inert solvents: Characteristics and applications. *Int. J. Biol. Macromol.* **2021**, *184*, 926−935.
(34) Chaouch, M.; Diouf, P. N.; Laghdir, A.; Yin, S. Bio-oil from whole-tree feedstock in resol-type phenolic resins. *J. Appl. Polym. Sci.* **2014**, *131*, No. 20170107.
(35) Tolesa, L. D.; Gupta, B. S.; Tiwikrama, A. H.; Wu, Y.-C.; Lee, M.-J. Alkali lignin degradation with aqueous ammonium-based ionic liquid solutions. *J. Cleaner Prod.* **2020**, *258*, 120724.
(36) Hälenius, F. Galaxite, $MnAl_2O_4$, a spectroscopic standard for tetrahedrally coordinated Mn^{2+} in oxygen-based mineral structures. *Am. Mineral.* **2007**, *92*, 1225−1231.
(37) Grosvenor, A. P.; Kobe, B. A.; McIntyre, N. S. Studies of the oxidation of iron by water vapour using X-ray photoelectron spectroscopy and QUASES. *Surf. Sci.* **2004**, *572*, 217−227.
(38) Kim, D.; Dhand, V.; Rhee, K.; Park, S. J. Study on the effect of silanization and improvement in the tensile behavior of graphene-chitosan-composite. *Polymers* **2015**, *7*, 527−551.
(39) David, L.; Bernard, S.; Gervais, C.; Miele, P.; Singh, G. Facile synthesis and high rate capability of silicon carbonitride/boron nitride composite with a sheet-like morphology. *J. Phys. Chem. C* **2015**, *119*, 2783−2791.
(40) Gunes, I. S.; Cao, F.; Jana, S. C. Evaluation of nanoparticulate fillers for development of shape memory polyurethane nanocomposites. *Polymer* **2008**, *49*, 2223−2234.
(41) Finster, J.; Heeg, J.; Klinkenberg, E. -D. Chemical and structural order in silicon oxynitrides by methods of surface physics. *Prog. Surf. Sci.* **1990**, *35*, 179−184.
(42) Bhandavat, R.; Singh, G.; Colombo, P. Synthesis, characterization, and high temperature stability of Si(B)CN-coated carbon nanotubes using a boron-modified poly(ureamethylvinyl)silazane chemistry. *J. Am. Ceram. Soc.* **2012**, *95*, 1536−1543.

https://doi.org/10.1021/acsomega.4c06375
ACS Omega 2025, 10, 13807−13815